Journal of Power Sources 244 (2013) 592–596

Contents lists available at SciVerse ScienceDirect

Journal of Power Sources

journal homepage: www.elsevier.com/locate/jpowsour

Short communication

High temperature defect chemistry in layered lithium transition-metal oxides based on first-principles calculations

Yukinori Koyama [a,*], Hajime Arai [a], Isao Tanaka [b], Yoshiharu Uchimoto [c], Zempachi Ogumi [a]

[a] Office of Society-Academia Collaboration for Innovation, Kyoto University, Gokasho, Uji, Kyoto 611-0011, Japan
[b] Department of Materials Science and Engineering, Graduate School of Engineering, Kyoto University, Yoshida, Sakyo, Kyoto 606-8501, Japan
[c] Graduate School of Human and Environment Studies, Kyoto University, Yoshida Nihon-matsu, Sakyo, Kyoto 606-8501, Japan

HIGHLIGHTS

- Defect chemistry at high temperatures in layered $LiMO_2$ is revealed.
- Antisite transition-metal ions are major defects in $LiCoO_2$ and $LiNiO_2$.
- Oxygen vacancy is major defect in $Li(Li_{1/3}Mn_{2/3})O_2$.
- Defect concentration is sensitive to synthesis conditions for $LiNiO_2$.

ARTICLE INFO

Article history:
Received 17 October 2012
Received in revised form
10 December 2012
Accepted 15 December 2012
Available online 21 January 2013

Keywords:
Defect chemistry
First-principles calculation
Lithium-ion battery
Electrode active material

ABSTRACT

Defect chemistry at high temperatures in layered lithium transition-metal oxides of $LiCoO_2$, $LiNiO_2$, and $Li(Li_{1/3}Mn_{2/3})O_2$ is investigated on the basis of first-principles calculations. The antisite transition-metal ions are the major defects in $LiCoO_2$ and $LiNiO_2$. However, the easy formation of the electron defect in $LiNiO_2$ leads to the preferential valence state of Ni_{Li}^{0} and thus to the $P_{O_2}^{-1/2}$ dependence of the defect concentration on the oxygen partial pressure. On the other hand, the formation of the electron defect as the accompaniment of the antisite cobalt ion in $LiCoO_2$ leads to the preferential valence state of Co_{Li}^{+} and the $P_{O_2}^{-1/4}$ dependence. The defect concentration is, therefore, more sensitive to the synthesis conditions for $LiNiO_2$ than that for $LiCoO_2$. $Li(Li_{1/3}Mn_{2/3})O_2$ with low defect concentrations can be easily synthesized at ambient oxygen partial pressures, although the concentration of the oxygen vacancy increases as oxygen partial presure decreases. The defect chemistry based on the first-principles calculations can provide quantitative information on the characteristics of electrode active materials as well as guides to their optimum synthesis conditions.

1. Introduction

Various lithium transition-metal oxides are examined as active materials of positive electrodes for lithium-ion batteries. Most of them are synthesized by solid-state reaction processes [1]. Point defects are formed at high temperatures in such synthesis processes, and some of them may remain in the samples owing to their slow diffusion at low temperatures. The residual defects are the cause of many properties of actual electrode active materials. For instance, $LiNiO_2$ always has excess nickel, and the excess nickel ion exists as an antisite defect at the lithium site. Although the amount of excess nickel should be small to obtain a large rechargeable capacity, which is an advantage of $LiNiO_2$ over $LiCoO_2$, the amount of the excess nickel is dependent on the synthesis conditions [2–4]. Therefore, knowledge of defect chemistry in electrode active materials at high temperatures is essential to optimize their synthesis conditions, and thus to improve performance of lithium-ion batteries.

Despite the importance of inquiry into defect chemistry in electrode active materials, it is difficult to accurately determine defect concentrations in lithium transition-metal oxides. Therefore, investigation on the defect chemistry based on theoretical calculations is expected. For this purpose, first-principles calculations based on density functional theory (DFT) is promising with consideration of chemical conditions and variety of valences of point defects [5]. The formation energies of the point defects that lead to nonstoichiometry are dependent on chemical conditions such as

* Corresponding author. Tel.: +81 774 38 4966.
E-mail addresses: koyama@saci.kyoto-u.ac.jp, y.koyama@at7.ecs.kyoto-u.ac.jp (Y. Koyama).

0378-7753/$ – see front matter © 2013 Elsevier B.V. All rights reserved.
http://dx.doi.org/10.1016/j.jpowsour.2012.12.127

oxygen partial pressure. Thus, the consideration of the chemical conditions is required for the evaluation of the defect concentrations. As transition-metal species can have variety of valences, point defects in transition-metal oxides may also have various valences. Hence, an electron defect, a hole defect, and point defects with different valences should be taken into account for evaluation of the defect concentrations.

We herein report an investigation of the defect chemistry at high temperatures in lithium transition-metal oxides of $LiMO_2$ (M = Co, Ni, and $Li_{1/3}Mn_{2/3}$) with an α-$NaFeO_2$-type layered structure based on systematic first-principles calculations. $LiCoO_2$ has the regular α-$NaFeO_2$-type structure. $LiNiO_2$ exhibits Jahn-Teller distortion, which causes a distortion from a rhombohedral lattice of the regular α-$NaFeO_2$-type to a monoclinic lattice [6]. $Li(Li_{1/3}Mn_{2/3})O_2$ exhibit a $[\sqrt{3} \times \sqrt{3}]R30^\circ$ superlattice in the $(Li_{1/3}Mn_{2/3})$ layers. We give and discuss the equilibrium concentrations of the point defects in these oxides at high temperatures and various oxygen partial pressures.

2. Calculation method

The formation energy of defect X at site A in valence state q is defined as

$$\Delta_f E(X_A^q) = E^{\mathrm{DFT}}(X_A^q) - E^{\mathrm{DFT}}(\mathrm{bulk}) - \sum_i \Delta n_i \mu_i + q\varepsilon_F \ , \quad (1)$$

where $E^{\mathrm{DFT}}(X_A^q)$ and $E^{\mathrm{DFT}}(\mathrm{bulk})$ are the energies of supercells obtained by DFT calculations with and without the defect X_A^q, respectively. Δn_i is the change in the number of atoms of species i, which has been added ($\Delta n_i > 0$) or removed ($\Delta n_i < 0$). μ_i is the atomic chemical potential of species i. ε_F is the Fermi energy. Note that $E^{\mathrm{DFT}}(X_A^q)$ and $E^{\mathrm{DFT}}(\mathrm{bulk})$ are, in principle, Gibbs free energies. However, the entropy and volume terms can be disregarded for solid phases. Under thermal equilibrium, the concentration of the defect X_A^q at temperature T can be obtained as

$$C(X_A^q) = C(A_A)\exp\left(-\frac{\Delta_f E(X_A^q)}{k_B T}\right), \quad (2)$$

where $C(A_A)$ and k_B are the concentration of site A without any defect and the Boltzmann constant, respectively. This estimation scheme assumes no interaction between defects and homogeneous distribution of the defects. The concentration is given per formula unit, in units of 1/f.u., in this paper. In the present work, point defects of vacancies (V_{Li}, V_M, and V_O), interstitial cations (Li_i and M_i) at the tetrahedral sites in the lithium layers, antisite cations (M_{Li} and Li_M), an electron defect (e^-), and a hole defect (h^+) were examined.

To represent a chemical condition of the $LiMO_2$ system under thermal equilibrium, one internal parameter (ε_F) and four external parameters (T, μ_{Li}, μ_M, and μ_O) exist. The Fermi energy was determined so that the system satisfied charge neutrality. Temperature and oxygen partial pressure were used as variables in this investigation. The atomic chemical potential of oxygen at temperature T and partial pressure P_{O_2} is given as

$$\mu_O = \frac{1}{2}G_{O_2} = \frac{1}{2}\left(E_{O_2}^{\mathrm{DFT}} + \left(G_{O_2}^0(T) - G_{O_2}^0(0\mathrm{K})\right) + k_B T \ln\left(\frac{P_{O_2}}{P^0}\right)\right), \quad (3)$$

where $E_{O_2}^{\mathrm{DFT}}$ is the energy of an O_2 molecule obtained by DFT calculation, corresponding to the Gibbs free energy at 0 K without the zero-point energy. $G_{O_2}^0$ is the Gibbs free energy of the gaseous O_2 phase under the standard pressure P^0 as a function of temperature, which is estimated by assuming the oxygen to be an ideal gas on the basis of experimental results [7]. The existence of the $LiMO_2$ phase requires a constraint on the chemical condition as

$$\mu_{Li} + \mu_M + 2\mu_O = E_{LiMO_2}^{\mathrm{DFT}}, \quad (4)$$

where $E_{LiMO_2}^{\mathrm{DFT}}$ is the energy of $LiMO_2$ obtained by DFT calculation. With these conditions, a single variable remains. In this investigation, the atomic chemical potential of lithium was set to be under equilibrium with Li_2O as

$$2\mu_{Li} + \mu_O = E_{Li_2O}^{\mathrm{DFT}}, \quad (5)$$

where $E_{Li_2O}^{\mathrm{DFT}}$ is the energy of Li_2O obtained by DFT calculation. This corresponds to setting the most lithium-rich condition during the synthesis to minimize lithium deficiency in the samples.

The defect energies were calculated using 144-atom ($Li_{36}M_{36}O_{72}$) supercells constructed by the expansion of the α-$NaFeO_2$-type unit cell by $2\sqrt{3} \times 2\sqrt{3}$ in the ab plane. Single defects were individually introduced into the supercells. Lattice constants were fixed at those of the pristine oxides. Atomic positions were optimized until the residual forces became less than 0.02 eV $Å^{-1}$. The electrostatic potentials of the charged supercells were corrected so that the electrostatic potentials at the farthest ions from the defects were the same as those in the pristine crystals [5,8,9]. The DFT calculations were performed using the plane-wave basis projected-augmented-wave (PAW) method implemented in the VASP code [10–12]. The plane-wave basis set was determined with a cutoff energy of 500 eV. The integral in the reciprocal space was evaluated by the Gaussian smearing technique with a smearing parameter of 0.1 eV and a $2 \times 2 \times 1$ mesh. The exchange-correlation interaction was treated by the generalized gradient approximation with the Hubbard model correction (GGA + U) [13,14]. A U parameter of 5 eV was commonly used for all the transition-metal species and valences in the present work.

3. Results and discussion

Fig. 1(a) illustrates the equilibrium concentrations of the point defects in $LiCoO_2$ as a function of temperature and oxygen partial pressure. Fig. 1(b)–(d) illustrate cross sections of Fig. 1(a) at $T = 1100$ K, $P_{O_2} = 0.2$ atm, and $P_{O_2} = 10^{-6}$ atm, respectively. The defect concentrations in the figures are the totals for each type of defects summed over all possible valences. The dominant defect in $LiCoO_2$ is the antisite cobalt ion at the lithium site (Co_{Li}). The oxygen vacancy (V_O) and the interstitial lithium ion (Li_i) are the minor defects at very high temperatures and low oxygen partial pressures. The calculated electronic states indicate that the antisite cobalt ion is in the divalent state with the high-spin configuration, whereas the regular cobalt ion is in the trivalent state with the low-spin configuration. The excess charge of the antisite cobalt ion is compensated by an electron defect as a small polaron (another divalent cobalt ion at the regular cobalt site).

Above 1000 K at 0.2 atm oxygen partial pressure, the electron defect is formed as an accompaniment of the defect formation reaction of the antisite cobalt ion as

$$LiCoO_2 \rightarrow Co_{Li}^+ + e^- + Li_2O + 1/2O_2. \quad (6)$$

Thus, the equilibrium concentrations of the antisite cobalt ion and the electron defect have $P_{O_2}^{-1/4}$ dependences, as shown in Fig. 1(b) at high oxygen partial pressures. At lower oxygen partial pressures, the antisite cobalt ion tends to be associated with an electron defect as the Co_{Li}^0 defect. Therefore, the total concentration of the antisite cobalt ion (Co_{Li}^+ and Co_{Li}^0) becomes more than the concentration of the electron defect as shown in Fig. 1(b) and (d).

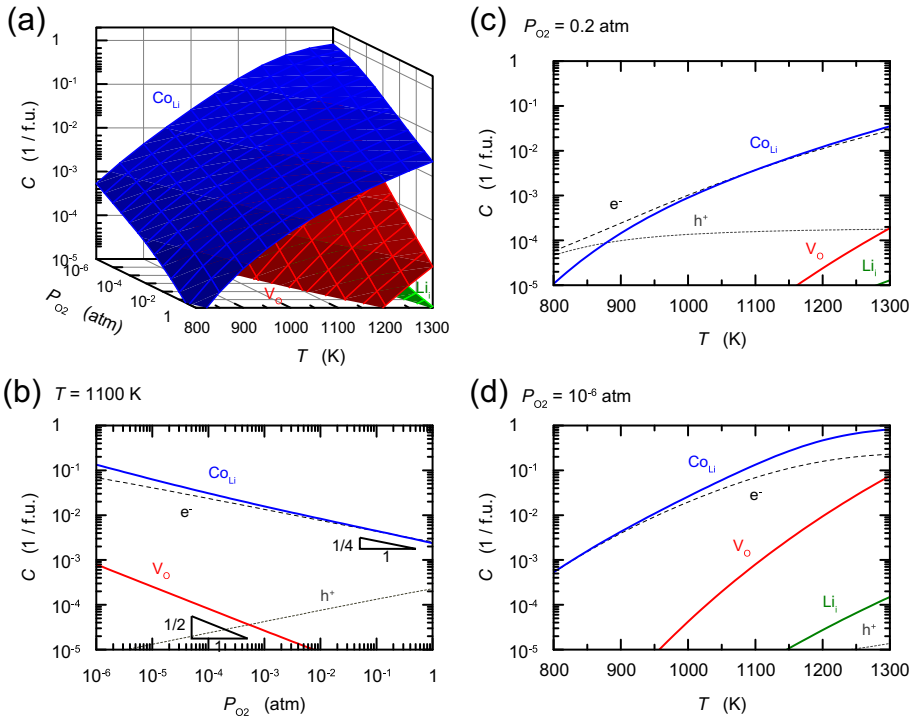

Fig. 1. (a) Equilibrium defect concentrations in $LiCoO_2$ as a function of temperature and oxygen partial pressure, and cross sections at (b) $T = 1100$ K, (c) $P_{O_2} = 0.2$ atm, and (d) $P_{O_2} = 10^{-6}$ atm.

The exponent of the concentration dependence of the total antisite cobalt ion on the oxygen partial pressure becomes greater than −1/4 as the oxygen partial pressure becomes lower. In contrast, the electron defect keeps the $P_{O_2}^{-1/4}$ dependence. The concentration of the hole defect is in relation to that of the electron by disproportionation reaction of

$$\text{Null} \rightarrow e^- + h^+. \tag{7}$$

Therefore, the concentration of the hole defect has a $P_{O_2}^{1/4}$ dependence, as shown in Fig. 1(b). The oxygen vacancy is mostly associated with two electrons, and thus in the zero valence state (V_O^0) in $LiCoO_2$. The formation reaction of the oxygen vacancy is

$$\text{Null} \rightarrow V_O^0 + 1/2\, O_2, \tag{8}$$

and the concentration of the oxygen vacancy has a $P_{O_2}^{-1/2}$ dependence.

Delmas and his coworkers reported that lithium-overstoichiometric $LiCoO_2$ slowly transformed to stoichiometric $LiCoO_2$ upon additional thermal treatments, suggesting that non-stoichiometric $LiCoO_2$ is thermodynamically unstable [15]. They also reported that highly stoichiometric $LiCoO_2$ was available through long thermal treatments [16]. These facts are consistent with the calculation results that the equilibrium defect concentrations in $LiCoO_2$ are low under ordinary synthesis conditions, i.e., at 800–900 °C under ambient atmosphere [1]. Approach to the thermal equilibrium under ordinary or oxidative atmosphere is important to obtain the very stoichiometric $LiCoO_2$, which is suggested to exhibit a less polarization [15] and a better reversibility for the first cycle [16] than the defective samples.

The equilibrium defect concentrations in $LiNiO_2$ are illustrated in Fig. 2(a) as a function of temperature and oxygen partial pressure. The cross sections at $T = 700$ K, $P_{O_2} = 0.2$ atm, and $P_{O_2} = 10^{-6}$ atm are shown in Fig. 2(b)–(d), respectively. The antisite nickel ion at the lithium site (Ni_{Li}) is the dominant defect in $LiNiO_2$. The oxygen vacancy and the interstitial lithium ion are the minor defects at high temperatures and low oxygen partial pressures. The types of the major and minor defects are the same as those in $LiCoO_2$. However, disproportionation of nickel ion of Eq. (7) easily occurs, and high concentrations of the electron and hole defects are expected. Therefore, the antisite nickel ion is mainly in the zero valence state (Ni_{Li}^0), which is a divalent nickel ion associated with an electron defect. Hence, the equilibrium defect concentration of the antisite nickel ion has a $P_{O_2}^{-1/2}$ dependence instead of $P_{O_2}^{-1/4}$, as shown in Fig. 2(b). The easy disproportionation also leads to weak dependences of the concentrations of the electron and hole defects on the oxygen partial pressure.

Because of the difference in the preferential valence state and greater dependence on oxygen partial pressure, the antisite defect is more easily formed in $LiNiO_2$ than that in $LiCoO_2$. This suggests that the concentration of the antisite defect is more sensitive to the oxygen partial pressure and temperature in the synthesis for $LiNiO_2$ than that for $LiCoO_2$. Oxidative atmosphere at low temperatures is, therefore, necessary to synthesize $LiNiO_2$ with fewer defects and less excess nickel. These calculation results are highly consistent with the experiments [2–4].

The equilibrium defect concentrations in $Li(Li_{1/3}Mn_{2/3})O_2$ are illustrated in Fig. 3(a) as a function of temperature and oxygen partial pressure. The cross sections at $T = 1100$ K, $P_{O_2} = 0.2$ atm, and $P_{O_2} = 10^{-6}$ atm are shown in Fig. 3(b)–(d), respectively. At oxygen partial pressure of 0.2 atm, the interstitial lithium ion is dominant at temperatures below 1000 K. On the other hand, the oxygen vacancy becomes dominant above 1100 K. At chemical conditions where the interstitial lithium ion is dominant, the electron defect is formed as an accompaniment of the formation of the interstitial lithium ion as

$$1/2\, Li_2O \rightarrow Li_i^+ + e^- + 1/4O_2. \tag{9}$$

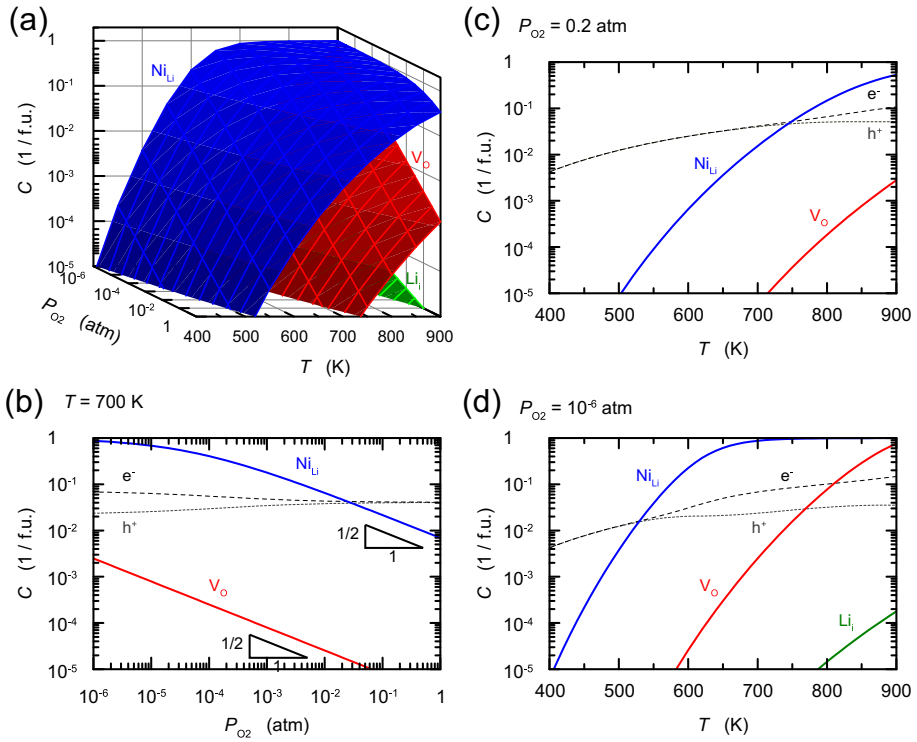

Fig. 2. (a) Equilibrium defect concentrations in $LiNiO_2$ as a function of temperature and oxygen partial pressure, and cross sections at (b) $T = 700$ K, (c) $P_{O_2} = 0.2$ atm, and (d) $P_{O_2} = 10^{-6}$ atm.

Thus, the equilibrium concentrations of the interstitial lithium ion and electron defect have $P_{O_2}^{-1/8}$ dependences. On the other hand, the oxygen vacancy is strongly associated with two electrons and thus in the zero valence state in $Li(Li_{1/3}Mn_{2/3})O_2$. Therefore, the oxygen vacancy is formed as the reaction of Eq. (8), and its concentration has a $P_{O_2}^{-1/2}$ dependence, as shown in Fig. 3(b). As the oxygen vacancy has greater dependence on the oxygen partial pressure than the interstitial lithium ion, the oxygen vacancy shows

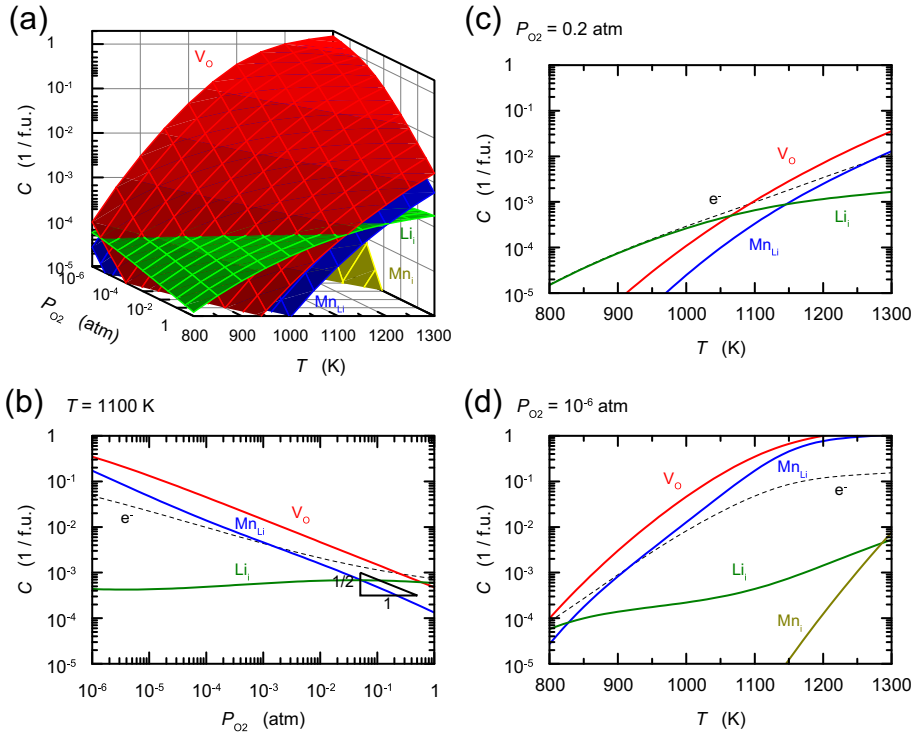

Fig. 3. (a) Equilibrium defect concentrations in $Li(Li_{1/3}Mn_{2/3})O_2$ as a function of temperature and oxygen partial pressure, and cross sections at (b) $T = 1100$ K, (c) $P_{O_2} = 0.2$ atm, and (d) $P_{O_2} = 10^{-6}$ atm.

a rapid increase in its concentration and exceeds the interstitial lithium ion at low oxygen partial pressures. In contrast to $LiCoO_2$ and $LiNiO_2$, the concentration of the oxygen vacancy is higher than that of the antisite manganese ion at the lithium site.

Despite intensive works in the world, $Li(Li_{1/3}Mn_{2/3})O_2$ and its derived materials are still immature as electrode active materials for lithium-ion batteries. Some groups reported that samples synthesized at lower temperature exhibited better electrochemical properties [17]. But, others reported similar electrochemical properties despite different synthesis temperatures [18]. Such inconsistency implies that the samples may be not under equilibrium conditions. As the optimum chemical composition (amount of the defects) is not clear for $Li(Li_{1/3}Mn_{2/3})O_2$ yet, the optimum synthesis condition is open to debate at this stage.

In this way, the defect concentrations under thermal equilibrium at high temperatures and various oxygen partial pressures were evaluated for the layered lithium transition-metal oxides based on first-principles calculations. The calculation results show the characteristics of these oxides in terms of defect chemistry, and they are highly consistent with the properties observed in experiments. The defect chemistry based on the first-principles calculations can provide quantitative information on the characteristics as well as guides to optimum synthesis conditions of electrode active materials.

4. Conclusions

Defect chemistry at high temperatures in the layered lithium transition-metal oxides is investigated on the basis of first-principles calculations. The antisite transition-metal ions are the major defects in $LiCoO_2$ and $LiNiO_2$. However, the easy formation of the electron defect in $LiNiO_2$ leads to the preferential zero valence state of the antisite nickel ion (Ni^0_{Li}) and thus the $P_{O_2}^{-1/2}$ dependence of the defect concentration on the oxygen partial pressure. In contrast, the formation of the electron defect as the accompaniment of the antisite cobalt ion in $LiCoO_2$ leads to the preferential valence state of Co^{+}_{Li} and the $P_{O_2}^{-1/4}$ dependence of the defect concentration. This leads to that the defect concentration is more sensitive to the synthesis conditions such as temperature and oxygen partial pressure for $LiNiO_2$ than that for $LiCoO_2$. $Li(Li_{1/3}Mn_{2/3})O_2$ with low defect concentrations can be easily synthesized at ambient oxygen partial pressures, although the concentration of the oxygen vacancy increases as oxygen partial pressure decreases. The defect chemistry based on the first-principles calculations can provide quantitative information on the characteristics of electrode active materials as well as guides to their optimum synthesis conditions.

Acknowledgments

This work was supported by the Research and Development Initiative for Scientific Innovation of New Generation Battery (RISING) project from New Energy and Industrial Technology Development Organization (NEDO), Japan.

References

[1] R. Koksbang, J. Barker, H. Shi, M.Y. Saidi, Solid State Ionics 84 (1996) 1.
[2] R. Kanno, H. Kubo, Y. Kawamoto, T. Kamiyama, F. Izumi, Y. Takeda, M. Takano, J. Solid State Chem. 110 (1994) 216.
[3] H. Arai, S. Okada, H. Ohtsuka, M. Ichimura, J. Yamaki, Solid State Ionics 80 (1995) 261.
[4] A. Rougier, P. Gravereau, C. Delmas, J. Electrochem. Soc. 143 (1996) 1168.
[5] K. Hoang, M. Johannes, Chem. Mater. 23 (2011) 3003.
[6] C.A. Marianetti, D. Morgan, G. Ceder, Phys. Rev. B 63 (2011) 224304.
[7] M.W. Chase Jr., NIST-JANAF Thermochemical Tables, , In: Journal of Physical and Chemical Reference Data Monographs Amer Inst of Physics, 1998.
[8] S. Poykko, M.J. Puska, R.M. Nieminen, Phys. Rev. B 53 (1996) 3813.
[9] C.G. Van de Walle, J. Neugebauer, J. Appl. Phys. 95 (2004) 3851.
[10] G. Kresse, J. Furthmuller, Phys. Rev. B 54 (1996) 11169.
[11] P.E. Blochl, Phys. Rev. B 50 (1994) 17953.
[12] G. Kresse, D. Joubert, Phys. Rev. B 59 (1999) 1758.
[13] J.P. Perdew, K. Burke, M. Ernzerhof, Phys. Rev. Lett. 77 (1996) 3865.
[14] S.L. Dudarev, G.A. Botton, S.Y. Savrasov, C.J. Humphreys, A.P. Sutton, Phys. Rev. B 57 (1998) 1505.
[15] S. Levasseur, M. Ménétrier, Y. Shao-Horn, L. Gautier, A. Audemer, G. Demazeau, A. Largeteau, C. Delmas, Chem. Mater. 15 (2003) 348.
[16] M. Ménétrier, D. Carlier, M. Blangero, C. Delmas, Electrochem. Solid-State Lett. 11 (2008) A179.
[17] Z.Q. Deng, A. Manthiram, J. Phys. Chem. C 115 (2011) 7097.
[18] H. Koga, L. Croguennec, P. Mannessiez, M. Ménétrier, F. Weill, L. Bourgeois, M. Duttine, E. Suard, C. Delmas, J. Phys. Chem. C 116 (2012) 13497.